Astron. Astrophys. 320, 273–286 (1997)

ASTRONOMY AND ASTROPHYSICS

Long-term spectroscopic monitoring of BA-type supergiants

III. Variability of photospheric lines⋆

A. Kaufer[1], O. Stahl[1], B. Wolf[1], A.W. Fullerton[4,5], Th. Gäng[1,3], C.A. Gummersbach[1], I. Jankovics[2], J. Kovács[2], H. Mandel[1], J. Peitz[1], Th. Rivinius[1], and Th. Szeifert[1]

[1] Landessternwarte Heidelberg-Königstuhl, D-69117 Heidelberg, Germany
[2] Gothard Astrophysical Observatory, H-9707 Szombathely, Hungary,
[3] STScI, Homewood Campus, 3700 San Martin Drive, Baltimore MD 21218, USA
[4] Max-Planck-Institut für Astrophysik, Karl-Schwarzschild-Str. 1, D-85740 Garching, Germany
[5] Universitäts-Sternwarte München, Scheinerstr. 1, D-81679 München, Germany

Received 5 September 1996 / Accepted 26 September 1996

Abstract. We obtained time series of spectra with high S/N and high resolution in wavelength and time of early-type A and late-type B supergiants (cf. Kaufer et al. 1996a, Paper I, and Kaufer et al. 1996b, Paper II for the analysis of the variability of the stellar envelopes). In this work we inspect the time variations of the numerous photospheric line profiles in the optical spectrum. We find complex cyclical variations of the radial velocities with a typical velocity dispersion of $\sigma \approx 3\,\mathrm{km\,s^{-1}}$. The corresponding equivalent-width variations are less than 1% of their mean if we assume a common modulation mechanism for both radial velocities and equivalent width. We do not find any depth dependence of the velocity fields in the metallic lines. For α Cyg the Balmer lines show an increase of the radial velocity from H27 to H8 by $3\,\mathrm{km\,s^{-1}}$, which is identified with the onset of the radially accelerating velocity field of the stellar wind. The CLEANed periodograms of the radial-velocity curves show the simultaneous excitation of multiple pulsation modes with periods longer and shorter than the estimated radial fundamental periods of the objects, which might indicate the excitation of non-radial and radial overtones, respectively. The analysis of the line-profile variations (LPV) of the photospheric line spectrum reveals prograde travelling features in the dynamical spectra. The travelling times of these features are in contradiction to the possible rotation periods of these extended, slowly rotating objects. Therefore, we suggest that these features should be identified with non-radial pulsation modes, possibly g-modes, of low order ($l = |m| \lesssim 5$).

Key words: stars: early-type, supergiants, emission-line, rotation, pulsation

Send offprint requests to:
A. Kaufer *e-mail*: A.Kaufer@lsw.uni-heidelberg.de

⋆ Based on observations collected at the European Southern Observatory at La Silla, Chile.

1. Introduction

Our extended spectroscopic monitoring of late B-type and early A-type supergiants (Kaufer et al. 1996a, Paper I, Kaufer et al. 1996b, Paper II; Stahl et al. 1995) has revealed for the first time the complexity of the circumstellar structures of these luminous objects. The time-series analysis of the Hα line-profile variability gave strong hints that the envelopes deviate from spherical symmetry. Further, based on time-scale arguments (Paper I) and the observation of reappearing absorption features in the circumstellar envelope (Paper II), the observed variability was attributed to rotation.

In this work we want to examine the line-profile variations (LPV) of the numerous photospheric lines in the $4000 - 6800$ Å wavelength range, which was covered by our spectrograph during all monitoring campaigns in the years from 1990 to 1995.

Abt (1957), Rosendhal & Wegner (1970a, 1970b), and Groth (1972) have found semiperiodic radial-velocity, line-strength, and width variations with typical time scales from 5 to 50 days and have discussed rotation and photospheric velocity fields like expansion, macroturbulence and depth-dependent microturbulence as possible line-broadening mechanisms.

The period analysis by Lucy (1976) of radial-velocity curves of α Cyg obtained in 1931/32 by Paddock (1935) revealed the simultaneous excitation of multiple pulsational modes including radial modes and low-order non-radial g modes. Due to the lack of comparable time series until now, this important result has not been verified for further BA-type supergiants.

In the following we want to use our large data set to fill this observational gap. We discuss the measured radial-velocity and line-strength variations and give the amplitudes of the variations and the frequency-spectra derived from the radial-velocity curves. Further, we use dynamical spectra to search for LPV characteristic for different types of velocity fields.

Table 1. The complete data set for all objects.

Object	sp	spectra/nights						$t_{\rm exp}$	S/N
		1990	1991	1992	1993	1994	1995	[min]	
HD 91619	B7 Iae	–	–	–	–	52/60	85/124	120	100
HD 34085 (β Ori)	B8 Iae	–	–	20/27	86/104	88/110	80/110	5–10	350–500
					4/26			10–40×10	300–1200
HD 96919	B9 Iae	–	–	–	83/116	102/130	83/124	60	150
HD 92207	A0 Iae	–	–	–	86/115	107/129	48/124	60	120
HD 100262	A2 Iae	–	–	–	–	98/130	46/124	60	150
HD 197345 (α Cyg)	A2 Iae	49/173	74/155	–	–	–	–	10	350
		–	–				1/1	120	1200

2. Data set

In the years from 1990 to 1995 we obtained extended time series of spectra in the wavelength range $4\,000 - 6\,800$ Å with high S/N and high resolution in wavelength ($\lambda/\Delta\lambda \approx 20\,000$) and time ($\Delta t \approx 1$ d) of the late-type B and early-type A supergiants HD 91619 (B7 Ia), β Ori (B8 Ia), HD 96919 (B9 Ia), HD 92207 (A0 Ia), HD 100262 (A2 Ia) and α Cyg (A2 Ia) with the FLASH spectrograph. This instrument was upgraded to the HEROS spectrograph between 1994 and 1995 (cf. Paper I and Paper II for a description of these instruments and the data reduction procedures). Table 1 gives a summary of the number of spectra obtained for each object in the different years including the recent observations of 1995. In addition, typical exposure times ($t_{\rm exp}$) and signal-to-noise ratios (S/N) in V are given.

Table 2. Number of lines for the cross-correlation templates, which cover the wavelength range from 4100 to 6700 Å. All Balmer lines are excluded. The three groups (w = weak, m = medium, s = strong) have been built according to the theoretical equivalent widths computed with the given stellar parameters and solar abundances for the Kurucz models and a microturbulence of $\xi_{\rm micro}$ = 15 km s^{-1} for the line-formation code.

sp	$T_{\rm eff}$ [K]	$\log g$	w $50-200$ mÅ	m $200-500$ mÅ	s >500 mÅ
B7	12000	1.6	66	20	1
B8	11000	1.4	68	27	4
A0	10000	1.4	109	30	10
A2	9000	1.2	127	53	13

3. Measurements

3.1. Cross-correlation technique

The optical spectra of BA-type supergiants display several hundred photospheric lines with equivalent widths $W_\lambda > 50$ mÅ, which are available for analysis of LPV.

To exploit this large number of lines, we use the cross-correlation of the individual spectra of a time series with a synthetic template spectrum. To do this, we construct a cross-correlation profile, which is a weighted mean of all photospheric lines included in the synthetic template. The template is constructed by computing LTE-model atmospheres (Kurucz 1979) for different stellar parameters, which roughly match the spectral types of the objects. With the LTE line-formation code of Baschek et al. (1966) in the version of Peytremann et al. (1967) the equivalent widths of all lines available in the line list of Kurucz & Peytremann (1975) are computed subsequently for solar abundances and a value of $\xi_{\rm micro}$ = 15 km s^{-1} for the microturbulence parameter in the wavelength range from $4100-6700$ Å. These computed equivalent widths are finally used as peak intensities of Dirac delta functions placed at the laboratory wavelengths given by the line list. All Balmer lines are excluded from the templates because of their obviously strong sensitivity to the wind variability, which is not the focus of this study. Fig. 1 shows the computed template spectra for the different spectral types listed in Table 2 together with the chosen stellar parameters for the model atmospheres. The increasing number of lines in the blue region (mainly due to FeII lines) for later spectral types is clearly seen.

To be sensitive to possible depth-dependent effects on the lines we have constructed for each spectral type three templates from three groups of lines with different strength. The group of weak lines (w) includes all lines from the spectrum synthesis with equivalent widths $50 < W_\lambda \leq 200$ mÅ, the medium strong group (m) the lines with $200 < W_\lambda \leq 500$ mÅ, and the strong group (s) all lines with $W_\lambda > 500$ mÅ. In Table 2 we give the respective number of lines in the templates of the w, m, and s group for the different stellar parameters. If we assume that on average weak lines form deeper in the atmosphere than strong lines, a possible depth dependence of, e.g., the radial velocities should be found (cf. below). With the three templates per spectral type we further receive three independent measurements of the LPV by using the cross-correlation method.

The cross-correlation method has several advantages: Basically this method constructs a high-S/N weighted mean profile with weights according to the relative line strengths. It is capable of handling the large number of lines available in the extended wavelength region of our instrument simultaneously. Compared to the red wavelength region of BA-type supergiants, the number of metallic lines in the blue is large (cf. Fig. 1), i.e., in the spectral region where the S/N is already lowered by the decreasing efficiency of our CCD. Therefore, this larger number of lines contributing to the cross-correlation profile can partially compensate for the lowered S/N. On the other hand

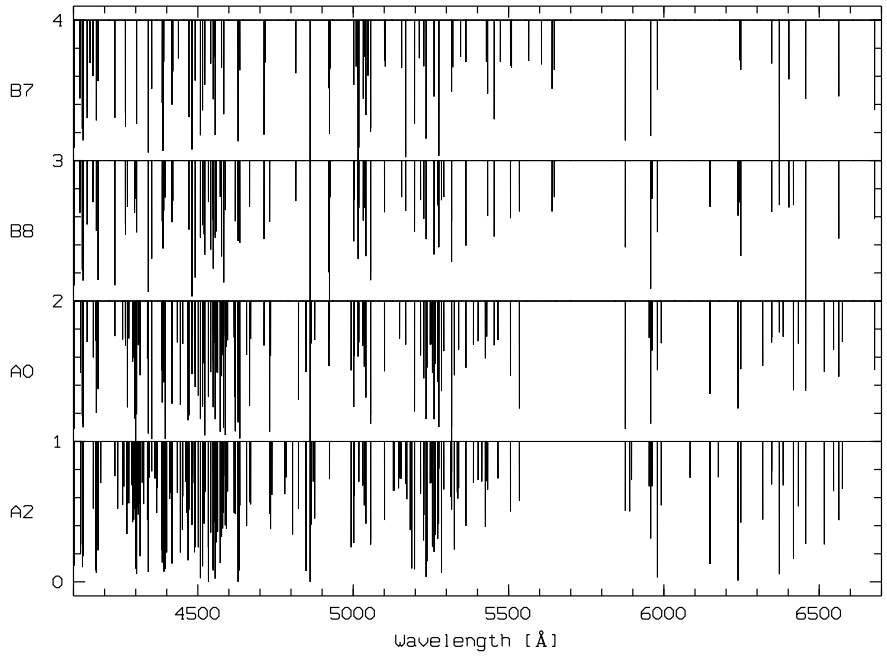

Fig. 1. The templates for the cross correlation. The quickly increasing number of mainly FeII lines towards later spectral types is nicely seen

a mismatch of the spectral type gives a rise of the noise in the cross-correlation spectrum because delta functions in the template which do not have lines as counterparts in the spectrum sample (noisy) continuum regions.

To test the performance of this method, we cross-correlated a template created from a sample of 16 weak telluric molecular oxygen lines ($2-10\%$ of the continuum) in the range from $6275-6300$ Å with the time series of β Ori of 1993. To account for the width of the stellar lines, the sharp telluric lines were broadened to a FWHM of about $50\,\mathrm{km\,s^{-1}}$, which leaves an extended line blend with 14 discernible components.

First, the positions, i.e., the radial velocities, of the correlation profiles were measured by fitting Gaussians. The radial velocities were then corrected to geocentric velocities because the spectra of the time series are in the heliocentric system. The time series with 86 spectra extends over 104 nights and shows a standard deviation of $\sigma_v = 0.35\,\mathrm{km\,s^{-1}}$ (1/10 pixel) and a peak-to-peak amplitude of $p\text{-}p\text{-}A = 1.7\,\mathrm{km\,s^{-1}}$. We assume these values to be an estimate for the radial-velocity accuracy reachable with our spectra and this measuring method.

Second, the intensities above the continuum of the unbroadened telluric correlation profiles in the geocentric system were integrated with fixed integration limits of $\pm 25\,\mathrm{km\,s^{-1}}$. Since the spectra of the time series were taken at airmasses between 1.1 and 3.0, each measured line strength had to be corrected by the respective value of the airmass at the mid-time of exposure. From the resulting, normally distributed line strengths a relative error (i.e., the standard deviation divided by the mean line strength) of 5% and a maximum error (i.e., the $p\text{-}p\text{-}A$ of the line strengths divided by the mean strength) of 29% was derived. We again take this value as an estimate for the reachable accuracy in measuring the line strengths from the cross-correlation profiles.

3.2. Depth dependencies

In this section we want to verify the assumption of the correlation of the equivalent width of a line and its depth of formation, which we want to use to probe the depth dependence of the atmosphere's structure (e.g. velocity fields). If the depth of line formation is not well correlated with the line strength as we assumed in our analysis, we would partially average out possible depth dependencies.

However, the depth of the formation of spectral lines is difficult to determine because spectral lines basically form throughout the whole photosphere. We computed an average depth of formation $\langle\tau_\lambda\rangle$ according to Achmad (1992) by a modified version of the line-formation program with

$$\langle\tau_\lambda\rangle = \frac{\int \tau \cdot \mathscr{C}_F^\ell(\tau)\cdot \mathrm{d}\tau}{\int \mathscr{C}_F^\ell(\tau)\cdot \mathrm{d}\tau}.$$

$\mathscr{C}_F^\ell$ is the contribution function to the emergent line radiation

$$\mathscr{C}_F^\ell(\tau) = \frac{\kappa_\ell}{\kappa_\mathrm{t}}.\mathscr{S}_\ell(\tau_\mathrm{t})E_2(\tau_\mathrm{t})$$

with $\mathscr{S}_\ell$ the line source function, E_2 the exponential integral, τ the reference optical depth of the atmosphere, and τ_t the monochromatic optical depth. Since we will measure mainly the radial velocities of the line cores (cf. Sect. 5) we computed $\langle\tau_\lambda\rangle$ only for the centers of the lines, i.e., at the laboratory wavelength.

Fig. 2 shows the correlation of the computed equivalent widths W_λ and the depth of formation $\langle\tau_\lambda\rangle$ for the A0-star model. The three groups of lines we selected for the further analysis are indicated. As expected we find a good correlation between $\log\langle\tau_\lambda\rangle$ and W_λ. The lines all form in the range $-2 < \log\langle\tau_\lambda\rangle < 0$, which according to the model atmosphere

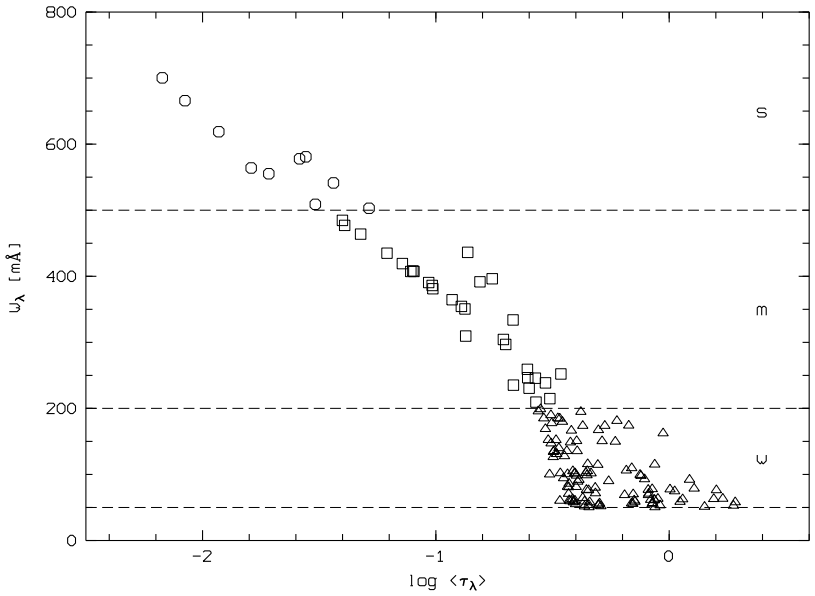

Fig. 2. Correlation of the average depth of formation $\langle\tau_\lambda\rangle$ of the core of a line and the equivalent width W_λ of the line for the A0-star model. The three groups of lines we formed according to their equivalent widths are indicated (w = triangles, m = squares, s = circles).

Table 3. Highest Balmer line H$m_{\rm max}$ observed in the averaged spectra of the program stars.

Object	*sp*	log g	H$m_{\rm max}$
HD 91619	B7 Ia	1.75	H25
HD 34085 (β Ori)	B8 Ia	1.67	H28
HD 96919	B9 Ia	1.50	H28
HD 92207	A0 Ia	1.32	H30
HD 100262	A2 Ia	1.46	H29
HD 197345 (α Cyg)	A2 Ia	1.54	H27

equals about 4.5 $R_\odot$ (for comparison: a typical stellar radius would be 120 $R_\odot$). It should be remembered that the Kurucz model atmospheres assume a plane-parallel stratification, which is probably not valid in this case anymore. But we also see that this method is of potential use to probe the depth structure of the atmosphere since the average depth of line formation extends over several percent of the stellar radius.

4. Balmer series

With the extension of the Heidelberg echelle spectrograph FLASH to HEROS in 1995, the wavelength region from 3500 – 4000 Å and therefore the complete Balmer series became reachable. Due to the low quantum efficiency of the CCD detector at that time, only the averaged spectra of the time series obtained 1995 at La Silla and a single well-exposed spectrum of α Cyg could be examined.

Table 3 gives for all program stars the highest discernible Balmer absorption line H$m_{\rm max}$ with m the number of the upper level of the Balmer transition $2 \rightarrow m$. The highest observable Balmer line is a measure for the width of the Balmer lines and therefore for the surface gravity log g. A comparison of H$m_{\rm max}$ with the values given for log g in Paper I verify the expected correlation. Since log g had to be derived from estimated masses and radii of the program stars this comparison was a valuable test for the reliability of our the stellar parameter estimation.

More important is the possibility of using the Balmer series to probe the transition zone from the stellar photosphere where the highest series members emerge to the base of the stellar envelope where the wind-sensitive Hα line is formed. As a first attempt to apply this powerful tool we show in Fig. 3 the Gaussian centered radial velocities of the line cores of the Balmer lines of α Cyg starting with Hγ up to the series limit at H27 plotted against the upper quantum number m.

The run of the radial velocities with m, i.e., the depth of formation of the line core, clearly shows a so-called 'progression' as expected for a radially accelerated velocity field. With the highest observable series members the radial velocities approach asymptotically the systemic velocity derived from the metal-line spectrum in Paper I. The increase of the velocity from H27 to H8 is almost linear and with a value of 3 km s^{-1} quite small, which might indicate that we really see the on-set of the wind-velocity field of α Cyg, which is expected to reach a terminal velocity of $v_\infty = -262$ km s^{-1} (cf. Paper I, Table 4).

A comparable study of the Balmer progression of the other program stars was not possible because the scatter of the measured radial velocities of $2 - 3$ km s^{-1} in the averaged spectra of the time series is comparable to the progression effect itself; the scatter in the individual spectra was even higher because of the low S/N in this spectral region.

5. Variations of photospheric lines

The photospheric lines of BA-type supergiants were known to be variable in radial velocity, line strength, and line width from previous studies (cf. Sect. 1).

We used the cross-correlation method described above to compute the time series of cross-correlation profiles for the three groups of lines. In the following we describe the time

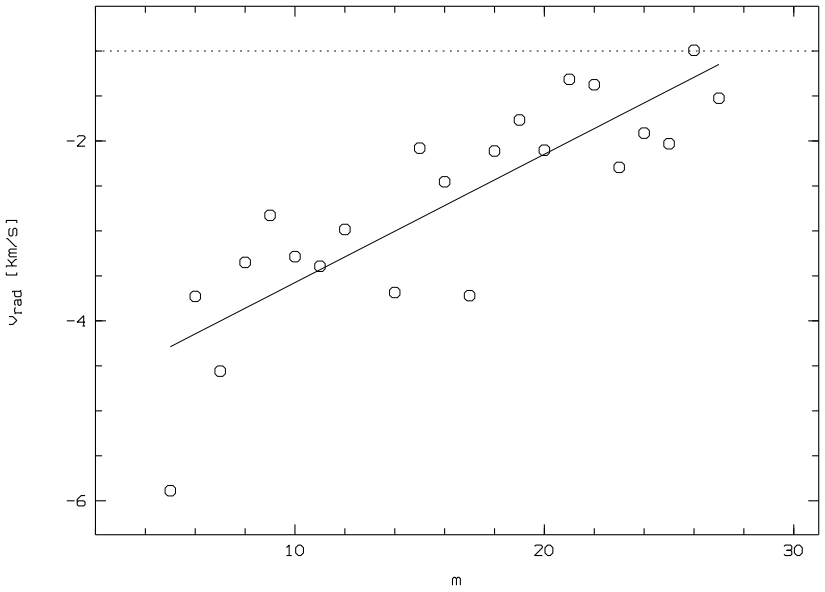

Fig. 3. The Balmer progression of α Cyg measured in a 2-hour exposure of the blue channel of HEROS at Heidelberg in 1995. The radial velocity of the line core is plotted against the upper quantum number m of the Balmer transition. The horizontal dashed line indicates the systemic velocity $v_{\rm sys} = -1\,{\rm km\,s^{-1}}$ derived in Paper I from the metal-line spectrum.

series of the therein measured radial-velocity and line-strength variations.

5.1. Radial-velocity variations

Radial velocities were measured by fitting Gaussians to the cross-correlation profiles. The use of Gaussians as model profiles is justified since all lines display symmetric profiles. However, in the case of HD 92207 we found weak blue wings in the line profiles of the strongest lines — a clear sign for a stronger mass-loss rate of this object, which is also supported by the strong P-Cygni profile displayed in Hα (cf. Paper I). In the cases of high-velocity absorptions (HVA) as described in Paper II, all program stars show blue and red asymmetries in the wings of the lines, too. Nevertheless, the centering of Gaussians is mostly sensitive to the line core, which in all our cases is symmetric.

Fig. 4 shows the cross-correlation radial velocity curve of HD 92207 in 1994 for s-, m-, and w-group lines. The three curves are almost identical in their shapes but also in very good agreement with respect to the mean radial velocity and the amplitudes of the variations. This holds for the radial-velocity curves of all other objects, too. Only the s-group curves are partially influenced by the above mentioned line asymmetries due to suddenly appearing HVA. Therefore, in Figs. 5 and 6 only the cross-correlation radial-velocity curves for all objects from the $200-500$ mÅ line group (m) are given. In Table 4 we have compiled the measured mean radial velocity $v_{\rm rad}$, the corresponding standard deviation σ, and the peak-to-peak amplitude (p-p-A) of the radial-velocity curves of the three groups of lines. The values derived for the α Cyg radial-velocity curves from the work of Paddock (1935) are also included.

Above, we have proposed to use the three groups of lines to search for a possible depth dependence of the radial-velocity variations. As can be seen in Table 4, the means of the radial velocities are within the estimated error of $0.4\,{\rm km\,s^{-1}}$ identical for the three groups. This also holds for the shapes of the radial-velocity curves of the three groups. Therefore, we conclude that the photospheric lines do not show depth-dependent velocity fields. Thus, the mean radial velocities give a good estimate of the systemic velocities $v_{\rm sys}$ of the objects. The values given for $v_{\rm sys}$ in Paper I, Table 4 are consistent with the mean radial velocities found by the cross-correlation analysis. The on-set of a radial acceleration was found in Sect. 4 from the

Table 4. Measurements from the radial-velocity curves of the three groups of lines: the mean radial velocity $v_{\rm rad}$, the corresponding standard deviation σ, and the peak-to-peak amplitude p-p-A. The values for α Cyg in 1931 and 1932 are derived from the published radial velocities (Paddock 1935), which were measured from w, m, and s-lines in the $4390-4630$ Å region

Object	year	mean $v_{\rm rad}$ [km s^{-1}]			σ [km s^{-1}]			p-p-A [km s^{-1}]		
		w	m	s	w	m	s	w	m	s
HD 91619	1994	−5.6	−6.7	−6.4	3.1	3.5	3.4	12.8	13.3	12.5
	1995	−4.5	−5.5	−7.2	3.2	3.8	3.7	12.7	16.4	17.2
HD 34085	1992	15.5	15.5	17.1	2.8	3.6	4.0	9.5	11.9	13.0
	1993	18.6	18.0	20.0	2.6	3.0	3.0	13.4	14.4	14.8
	1994	16.0	15.8	16.9	2.0	2.3	2.5	10.0	11.0	11.8
	1995	18.0	17.0	17.2	2.6	2.8	2.7	14.5	15.9	14.8
HD 96919	1993	−25.2	−24.6	−22.0	2.8	3.2	3.6	11.4	15.1	14.3
	1994	−25.1	−24.4	−22.0	3.1	3.2	3.8	18.4	19.2	19.3
	1995	−22.8	−22.7	−21.9	2.8	2.9	3.3	11.5	10.7	12.7
HD 92207	1993	−16.8	−17.8	−17.8	2.9	2.9	3.2	12.2	11.3	15.5
	1994	−17.8	−18.3	−17.9	3.9	4.4	4.6	17.0	17.7	18.0
	1995	−17.0	−15.9	−15.3	3.5	3.8	4.0	14.7	15.2	15.7
HD 100262	1994	−17.4	−17.9	−17.1	1.7	1.8	1.9	7.8	8.6	10.0
	1995	−13.9	−12.9	−12.9	1.6	1.7	1.7	6.4	7.2	7.1
HD 197345	1990	−0.9	−1.1	0.1	3.0	3.1	3.1	10.8	10.9	10.9
	1991	−2.3	−2.6	−1.9	2.2	2.1	2.1	9.8	8.6	8.3
	1931		−4.2			−2.0			−9.9	
	1932		−2.2			−2.7			−11.4	

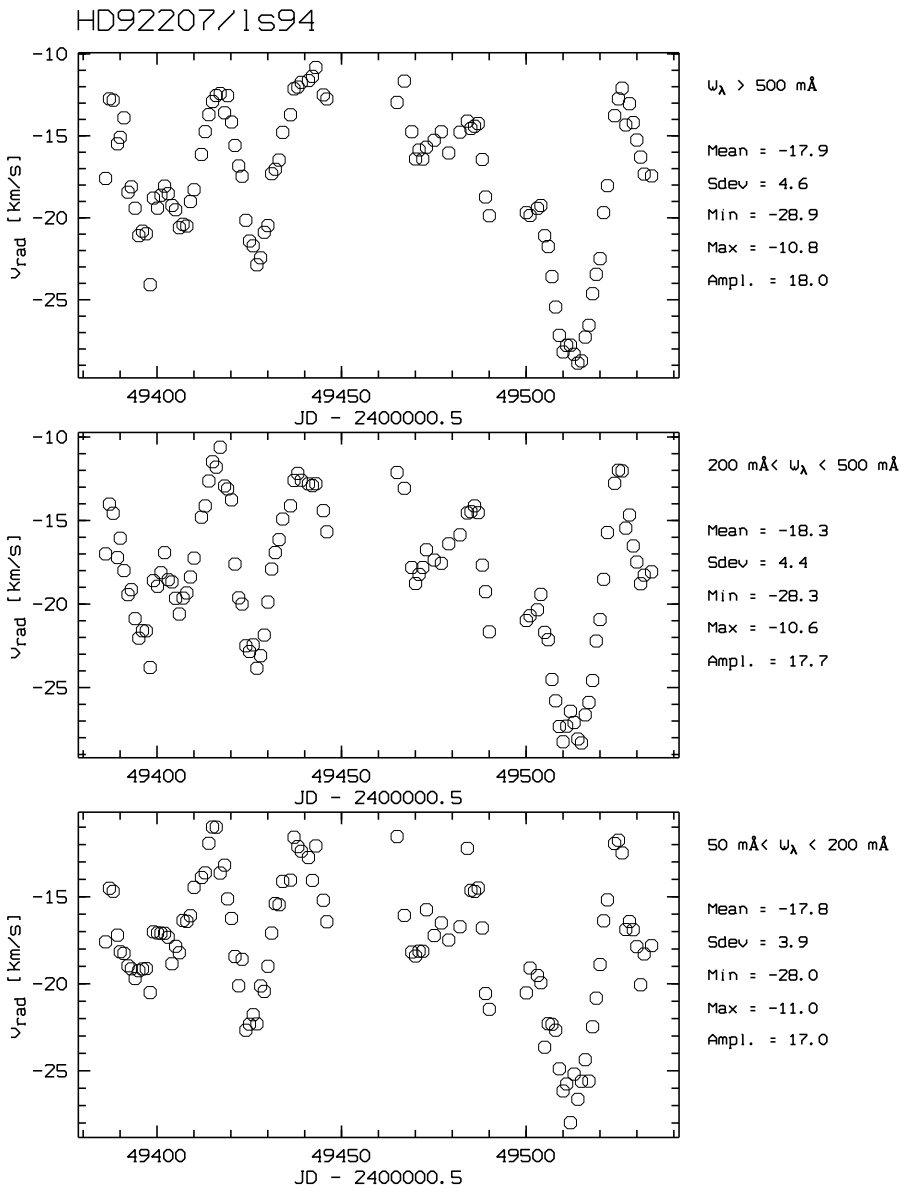

Fig. 4. Radial velocity variations of the s-, m-, and w-group lines of HD 92207 in 1994. The radial-velocity curves correspond to the three depths of line formation defined by the s, m, and w group but are in very good agreement in their shapes, their mean radial velocity, and their amplitudes. No depth dependence can be detected.

Balmer progression of α Cyg. It should be noted that the computed depths of formation $\langle\tau_\lambda\rangle$ of the very strong Balmer lines give values clearly beyond the lines of the s group, i.e., they are formed in the transition zone between photosphere and wind.

Variable depth-dependent velocity fields have been reported by several authors (e.g. by Chentsov & Snezhko 1971 for β Ori) from measurements of radial velocities of single, selected lines. In this method the laboratory wavelengths of the lines to compute the velocities are crucial (1 km s^{-1} equals 0.02 Å at 6000 Å). In the case of line blends with unresolved contributions from weak lines, an effective laboratory wavelength has to be found, which requires precise knowledge of the relative line strengths. Note that this need is automatically fulfilled by the synthetic templates in the cross-correlation method, which also averages out the uncertainties in laboratory wavelengths by the large number of lines in the templates.

The strongest gradients in the published depth-dependent velocity fields are found for the transition from photospheric lines to the lines of the Balmer series. As was shown in Sect. 4 the higher series members of the Balmer lines are influenced by the onset of the wind-velocity field. Therefore, the Balmer series is of the most potential use to study the transition from photospheric to wind variability in a homogeneous set of lines. A direct comparison of the dynamical spectra of the highest and lowest members of the Balmer series does not reveal any causality in the sense that photospheric variations could be followed into the wind as disturbances. This can also be seen in Table 4: the lines of the s group are clearly influenced by the appearance of extreme wind events like the HVA but not the lines of the m and w group. Therefore, we will first examine the photospheric variations independently of the wind variations.

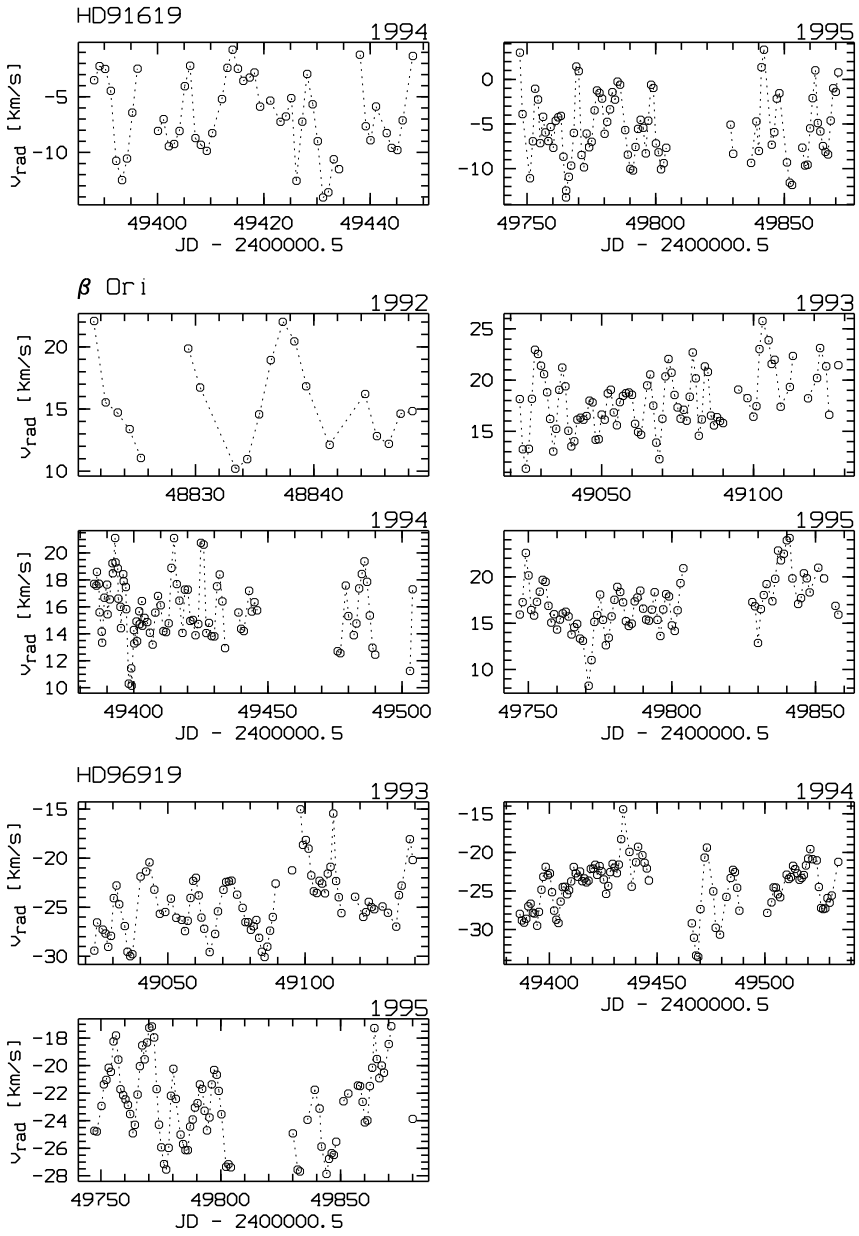

Fig. 5. Radial velocity variations of the m-group lines in HD 91619, β Ori, and HD 96919

The standard deviations σ of the radial-velocity variations in Table 4, which are a good statistical measure for the amplitudes of variations, are consistent for each object from year to year. The σs are in the range from $1.5 - 4.5\,\mathrm{km\,s^{-1}}$ with a clear maximum around $3\,\mathrm{km\,s^{-1}}$. The σs slightly increase from the w to the s lines, which is due to the increasing influence of the wind variability with the increasing line strengths. No dependence of the σs on the spectral type is seen.

Obviously there is no strict periodicity involved in the radial-velocity variations as presented in Figs. 5 and 6, rather, multiple time scales are involved. The time scales are of the same order as given in the literature and cover semiperiods from days to months. For a more precise determination of these time scales we applied the CLEAN technique described in Paper I (for the analysis of the equivalent-width curves of Hα) to the radial-velocity curves. We searched for significant periods in the frequency range from $0.01 - 1\,\mathrm{days^{-1}}$, which represents the typical length and sampling rate of our time series. The iterative removal of the peaks in the periodograms was terminated once all the peaks above a level of significance for a 99.5% probability ($\approx 3\sigma$) had been detected.

With the three groups of lines (w, m, and s) in the cross-correlation templates we obtained three independent measurements of the radial-velocity curves. Therefore, we perform the period analysis for the three curves independently, too, and reject periods that do not show up in at least two of the three periodograms with a 3σ significance.

The resulting CLEANed frequencies are shown in Fig. 7 for all program stars in the different years. The different symbols stand for the different groups of lines (triangles = w,

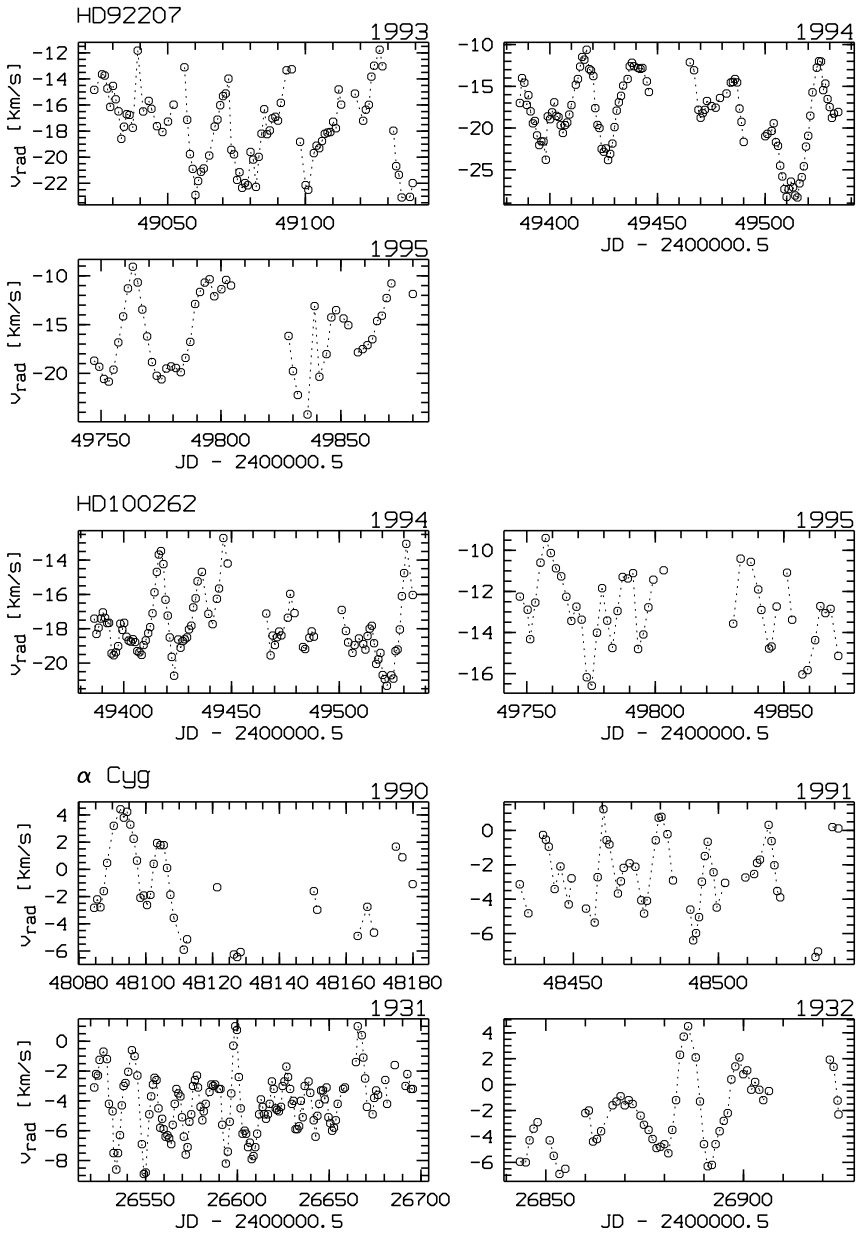

Fig. 6. Same as Fig. 5 but for HD 92207, HD 100262 and α Cyg. For α Cyg in addition to our observations, the measurements of Paddock (1935) in 1931 and 1932 are shown

squares = m, circles = s); the size of the symbols represent the power (i.e., the significance) of the respective peaks in the periodograms. Theoretical radial-fundamental pulsation periods computed according to Lovy et al. (1984) for a pulsation constant of $\log Q = -1.4$ are indicated by horizontal dashed lines.

The multiple frequencies measured with the described CLEAN method are for all program stars clearly shorter than the time scales derived from the Hα-equivalent curves with the same method in Paper I. The Hα time scales could be characterized by a single dominant period, which was connected to rotational modulation of the circumstellar envelope. The multiple time scales derived from the radial-velocity curves of photospheric lines display a completely different character. The derived frequencies are grouped around the estimated radial-fundamental pulsation periods $P_{\rm rad,fund}$ and the periods with maximum power are fairly compatible with the radial fundamental. The period spectra always display periods shorter as well as longer than $P_{\rm rad,fund}$. This is consistent with the period analysis of α Cyg by Lucy (1976). Periods with $P > P_{\rm rad,fund}$ suggest the excitation of non-radial pulsation modes, presumably g-modes of low order ($m \approx 1, 2, \ldots$). On the other hand, periods with $P < P_{\rm rad,fund}$ could be attributed to the first overtones of the radial pulsation modes.

The interpretation of the photospheric variations as velocity fields caused by pulsation is tempting but also questionable due to the fact that the period spectra are not stable from one observation run to the next, but new periods show up while others disappear. In a pulsation model this observational fact could be explained by a period spectrum which is basically rich in the

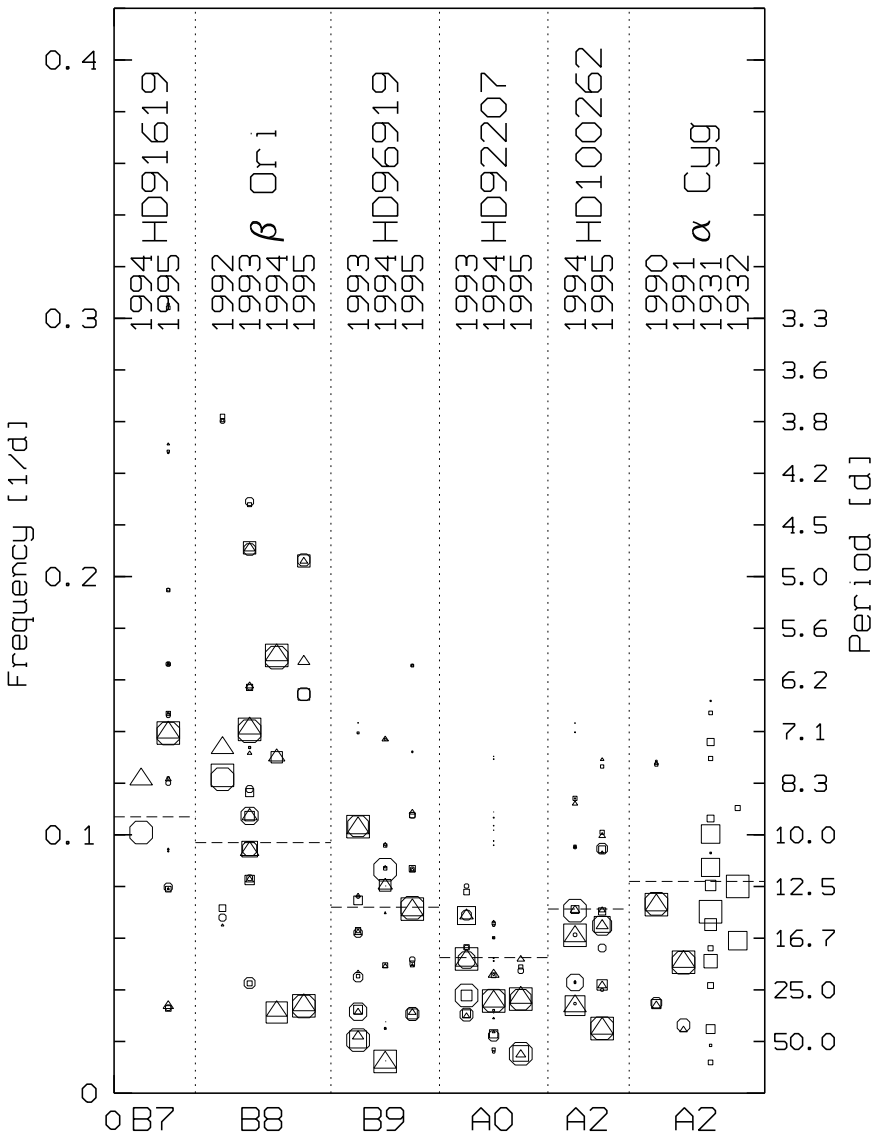

Fig. 7. CLEANed frequencies from the radial-velocities curves, which were measured with the cross-correlation method. For β Ori in 1992 and HD 100262 in 1995 frequencies with a 2σ probability are shown, all the others are with 3σ. The different symbols stand for the different groups of lines (triangles = w, squares = m, circles = s); the size of the symbols represent the power (the significance) of the respective peaks in the periodograms. The horizontal dashed lines give $P_{\rm rad,fund}$ for $\log Q = -1.4$.

number of modes but excitation is selective, i.e., only few modes are excited simultaneously and later disappear again.

In the mass and temperature range of the BA-type supergiants only few excitation mechanisms for pulsation have been found. Based on a linear non-adiabatic stability analysis Gautschy (1992) postulated the excitation of so-called strange modes. But with this mechanism (cf. Kiriakidis et al. 1993 for radial modes and Mehren 1994 for non-radial modes) pulsational instabilities for BA-type supergiants are only found for reduced masses ($\approx 6\,M_\odot$ for α Cyg, Gautschy 1992) or very high quantum numbers ($l \approx 50$ for a stellar mass of $20\,M_\odot$, Mehren 1994), which are not observable with current spectroscopic methods as global oscillations in the integrated light .

5.2. Line-strength variations

The line strengths were measured in the time series by integrating the cross-correlation profiles in the range $\pm 150\,\mathrm{km\,s^{-1}}$ about the respective systemic velocity of the object. Table 5 summarizes the results of the line-strength measurements. The relative variation (i.e., the standard deviation of the measurements divided by the mean line strength) and the maximum variation (i.e., the p-p-A of the measurements divided by the mean line strength) are given. Both, relative and maximum variation are mostly within the estimated reachable accuracy of the line-strength measurements, i.e., 5 and 29%, respectively. Therefore, we conclude that the line-strength variations found by our measurements are not significant and must be below a 5% level. This is further supported by the time-series analyses of the line-strength curves with our CLEAN method, which finds *no* significant periods above a 3σ level of significance. If

Table 5. Amplitudes of variations from the line-strength curves of the three groups of lines: rel.var. is the standard deviation of the line-strength variations relative to the mean line strength, max.var. the p-p-A of the line-strength variations relative to the mean line strength, and upp.lim. an upper limit of the line-strength variations derived from the power spectra with the periods from the radial-velocity curves.

Object	year	rel.var. [%]			max.var. [%]			upp.lim. [%]
		w	m	s	w	m	s	
HD 91619	1994	7.4	5.1	4.6	31.6	19.7	18.2	1.0
	1995	5.9	4.0	5.6	28.6	19.7	23.3	1.0
HD 34085	1992	1.2	1.8	2.5	4.3	6.3	9.1	0.6
	1993	2.8	3.3	1.7	11.6	14.5	7.1	0.5
	1994	2.6	2.2	2.2	10.8	9.4	9.7	0.5
	1995	2.8	1.8	2.4	13.7	7.8	8.7	0.4
HD 96919	1993	7.3	5.3	3.5	32.2	21.0	15.0	1.0
	1994	5.0	3.3	2.9	22.1	15.3	12.8	0.7
	1995	3.5	5.1	28.6	16.4	20.3	110.6	0.6
HD 92207	1993	8.4	7.9	5.3	33.4	36.7	21.6	1.0
	1994	10.3	5.5	4.3	41.7	25.6	20.8	1.0
	1995	4.1	3.0	2.4	19.0	10.9	12.0	0.6
HD 100262	1994	2.5	2.1	2.1	10.9	8.5	8.9	0.5
	1995	2.2	2.6	2.4	9.0	12.3	8.9	0.6
HD 197345	1990	2.4	1.3	1.1	8.5	5.9	4.5	0.5
	1991	3.8	3.3	2.8	15.9	12.8	10.3	0.6

line-strength variations did exist, they would be expected to be correlated e.g. to the radial-velocity variations and to show the same frequency spectrum. To tighten the upper limits of the line-strength variations, we then measured the relative amplitudes of the variations in the computed power spectra (the power is proportional to the amplitude squared) at the frequencies found by the radial-velocity analyses described above. The results are given in the last column of Table 5. If a common mechanism for the radial-velocity and the line-strength variations is assumed, the upper limits for the line-strength variations can be fixed to $0.5 - 1.0\%$.

This result implies some interesting constraints for the nature of the photospheric variability mechanism of the BA-type supergiants. The LPV of the photospheric lines are basically caused by a redistribution of the flux within the line profile and are not coupled to variations of the overall line strength. Such a behaviour would be expected for photospheric macroscopic velocity fields which do not lead to secondary effects such as temperature variations or variations of the local gravity. These requirements are compatible with non-radial pulsations with small amplitudes (Unno et al. 1979).

5.3. Photometric variability

Further hints concerning the nature of the photospheric variations can be found from photometric observations of the stellar continuum. Unfortunately, no photometry could be obtained strictly simultaneous with the spectroscopic time series. In the course of the LTPV (long-term photometry of variable stars) program (Sterken 1983) one of the program stars, HD 92207, was monitored in the $uvby$-Strömgren system over a time span of 8 years ($1986 - 1994$). The observations were mainly carried out at the Danish 50-cm telescope at La Silla, Chile.

Fig. 8, left, shows the complete y lightcurve differential to one of the comparison stars. Cyclical changes of the brightness are clearly discernible – unfortunately, the time scales of the light variations are several weeks, which is comparable to the typical length of an LTPV observing campaign. The maximum amplitude of all the recorded light variations is 0.12 mag and no long-term trends can be seen. The measured color variations $b-y$ and $u-b$ are 0.03 mag, the same order as the color variations of the comparison stars and therefore presumably not significant.

Fig. 8, right, shows the Scargle periodogram of the y lightcurve of HD 92207. The CLEANed periods with a 3σ significance have been determined to be 148, 62, 44, 27, and 21 d with comparable power in all periods. The period of 148 d lies close to the rotational period $P_{\rm rot}$ derived in Paper I ($P_{\rm rot}/\sin i = 160$ d). The length of the spectroscopic observation runs is of the same order and therefore this long period was not found in these data sets. But the other four periods are present in the radial-velocity curves, where the dominant period was found to be $P_v = 27.3$ d with an amplitude of $A_v = 3.0\,{\rm km\,s^{-1}}$ as average of three years (1993 = 26.4 d, $2.0\,{\rm km\,s^{-1}}$; 1994 = 28.0 d, $3.6\,{\rm km\,s^{-1}}$; 1995 = 27.6 d, $3.5\,{\rm km\,s^{-1}}$). The photometric amplitude of the frequency component with a period of 27 d equals $\Delta m = 0.01$ mag.

If we assume that the light variations in HD 92207 are solely caused by variations of the stellar radius (which seems to be a reasonable assumption since the color variations are insignificant), the brightness amplitude $\Delta m_{\rm rad}$ computes as

$$\Delta m_{\rm rad} = 5 \cdot \log \left(1 + 0.02 \, \frac{P_v[{\rm d}]\, A_v[{\rm km\,s^{-1}}]}{R_\star[{\rm R}_\odot]} \right).$$

With a radius for HD 92207 of $R_\star = 157\,{\rm R}_\odot$ and the assumption that the 27 d-period is caused by a radial pulsation, we obtain a photometric amplitude of $\Delta m_{\rm rad} = 0.02$ mag. This value is consistent with the measured photometric amplitude of 0.01 mag, once allowance is made for the assumptions. Therefore, we conclude that the photometric variability of HD 92207 (and probably all BA-type supergiants) is related to radius variations, which are measurable in the radial-velocity curves.

5.4. Line-profile variations

The high quality of our spectroscopic data permits the line-profile variations (LPV) to be analyzed directly as function of time. This is indispensable to trace down the origins of variability in the integrated measures like radial velocity and equivalent width to a physical mechanism.

In a first step we want to examine the distribution of the LPV across the profile. For this purpose we computed the temporal variance spectra (TVS, cf. Fullerton et al. 1996 for a detailed description of the method), which so far had been used for the analysis of the Hα variability only (cf. Paper I). Fig. 9 shows the $({\rm TVS})^{1/2}$ in the region of the photospheric Si IIλ6347 line,

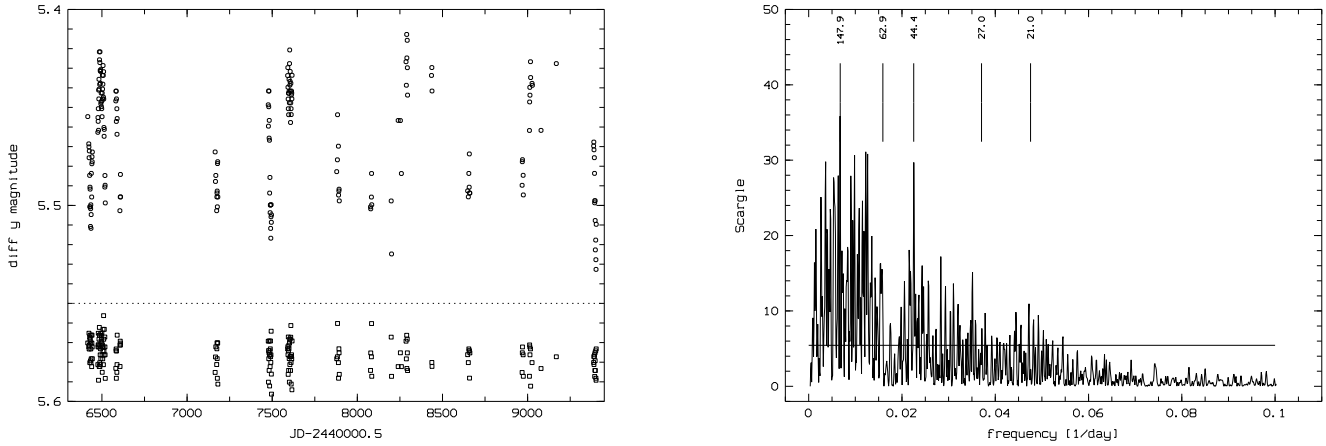

Fig. 8. Left: differential lightcurve in y measured by the LTPV program for HD 92207. Below, the differences of the two comparison stars are shown (arbitrarily shifted). Right: the corresponding periodogram. The CLEANed periods for a 3σ probability are indicated.

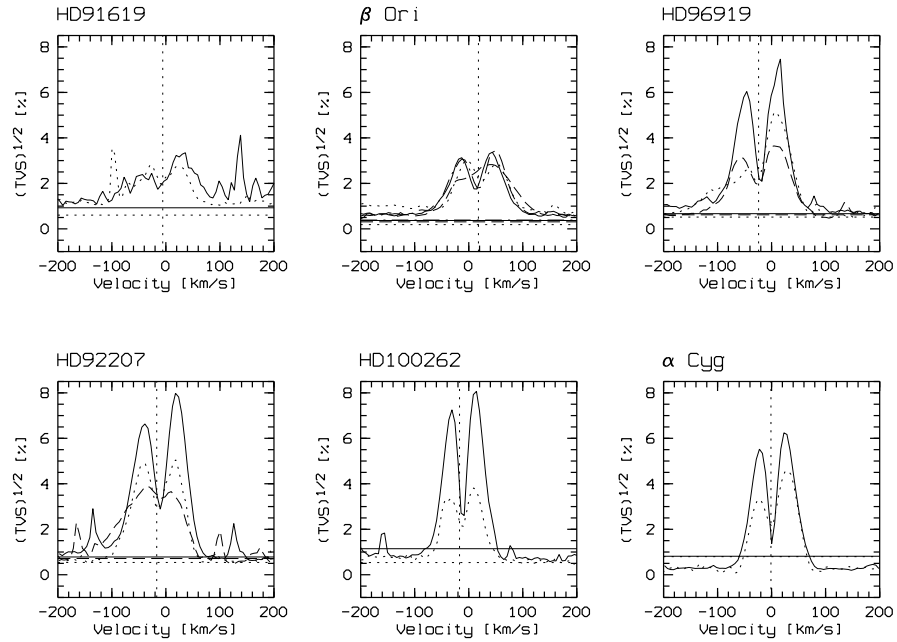

Fig. 9. TVS of Si IIλ6347. (1992 = dash-dotted, 1993 = short-dashed, 1990,1994 = full, 1991,1995 = dotted lines). Further, the levels of significance for a 95% probability are indicated by horizontal lines. The vertical dashed lines indicate the systemic velocities $v_{\rm sys}$ of the objects as given in Paper I, Table 4.

which is a comparatively strong line for all spectral types under consideration that falls in the best-exposed wavelength region of the spectrograph and therefore appears to be well-suited for this pilot study.

The TVS of the Si IIλ6347 line display a characteristic distribution of the variability over the line profile, i.e., a double-peaked structure with the maxima of the peaks at the positions of the maximum gradients of the photospheric line profile. This indicates that the variability happens mainly in the wings of the line profiles but is non-negligible at the line core. Assuming a pulsational nature for the observed LPV, this appearance of the TVS is indicative for a simultaneous existence of radial and non-radial modes, the latter giving the main contribution to the TVS at the line core due to travelling bumps crossing the complete profile. Radial modes only contribute in the line wings where the gradient in the line profile is strongest. Therefore, we have hints for the simultaneous presence of radial and non-radial velocity fields in the photospheres of BA-type supergiants from the TVS and the period spectra.

The characteristics of the LPV are displayed best as dynamical spectra of the quotient spectra of the time series, i.e., the individual spectra divided by the weighted average of all contributing spectra. The superposition of multiple pulsation modes leads to complex LPV. Consistent with the large number of frequency components (typically $5-10$ significant periods) derived from the periodograms of the radial-velocity curves, the dynamical quotient spectra of the program stars show very complex LPV where individual characteristics of radial or non-radial modes are not discernible.

Therefore, we present in Fig. 10 the dynamical quotient spectrum of the Si IIλ6347 line of HD 92207 in 1994 – the year

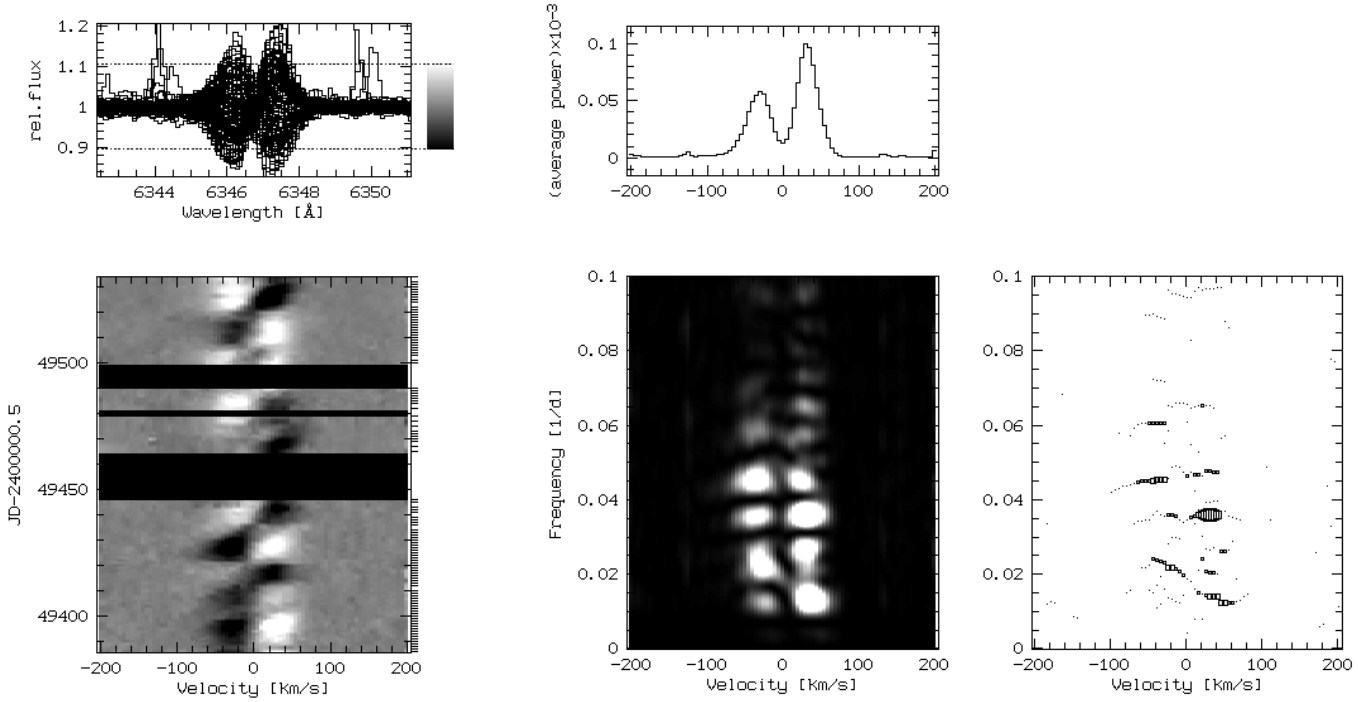

Fig. 10. Left: dynamical quotient spectrum of the Si IIλ6347 line of HD 92207 in 1994. Note that the spectra were shifted to laboratory wavelengths using a systemic velocity of $v_{\rm sys} = -17\,{\rm km\,s^{-1}}$ for HD 92207 (cf. Paper I, Table 4). Middle: the corresponding two-dimensional power spectrum. Right: the CLEANed frequencies across the line profile for a 99.5% significance.

when this objects showed only one dominant period in the radial velocities (cf. Fig. 7) with a period length of 27 d.

In this case the LPV are quite periodic, as indicated in the dynamical spectrum by regularly alternating pseudo absorptions and pseudo emissions. Furthermore, the intensity distribution over the line profile in the quotient spectra (left) and in the two-dimensional power spectrum (middle) verifies the preferred variability in the line wings which is indicative for strong radial contributions of the velocity field. Apart from that, variability is also observed at the line core mainly caused by pseudo absorption and pseudo emission features travelling across the line profile from blue to red as expected for non-radial contributions.

A very good example for features migrating across the line profiles was observed in HD 92207 in 1993 and is shown as dynamical quotient spectrum in Fig. 11, left. The travelling time of the components across the line profile is about 27 d. If we want to attribute the corresponding structure on the stellar surface to a corotating feature, the rotational period of HD 92207 would be 54 d. As a lower limit for the rotational period of this star we determined in Paper I a value of 55 d from its break-up velocity; an upper limit was estimated from the widths of the line profiles with $P_{\rm rot}/\sin i = 160$ d. Solely from the fact that we observe travelling features we can expect to view this star preferably equator-on than pole-on, which would make an explication of the observed 54 d period by strict corotation implausible. On the other hand, this would imply that the observed surface structure must have an additional azimuthal velocity component – a distinctive feature of any non-radial pulsation since its patterns are running around the star's surface. From the direction of the observed travelling features (i.e., from blue to red) we can determine the non-radial wave to travel around the star's surface in the sense of rotation, i.e., prograde. Since at one point of time always one emission component is visible together with one absorption component, the number of meridional sectors can be estimated to $|m| \approx 2$.

In Fig. 11, right, we present a simulation of the LPV caused by a non-radial velocity field following the equations (7.1) of Unno et al. (1979) with the stellar parameters of HD 92207 from Table 4 in Paper I and $\sin i = 1$, $l = -m = 2$, $\sigma_{\rm nrp} = \frac{2\pi}{60}\,{\rm d}^{-1}$. Both dynamical spectra basically show a coincidence in their temporal behaviour and the appearance and number of the pseudo absorption and emission components.

It should be emphasized again that such clear pulsation-like structures in the LPV as these are observed rarely in the time series of the BA-type supergiants. Generally, they are hidden in the complex appearance of the LPV patterns due to the multi-periodicity of the photospheric velocity fields. Therefore, we only can summarize for all further program stars that travelling features are discernible in the LPV and always show the same incompatibility of their travelling time across the profile and strict corotation.

6. Summary and conclusions

In this paper we have concentrated the analysis of our extended time series of high-resolution spectra of BA-type supergiants on

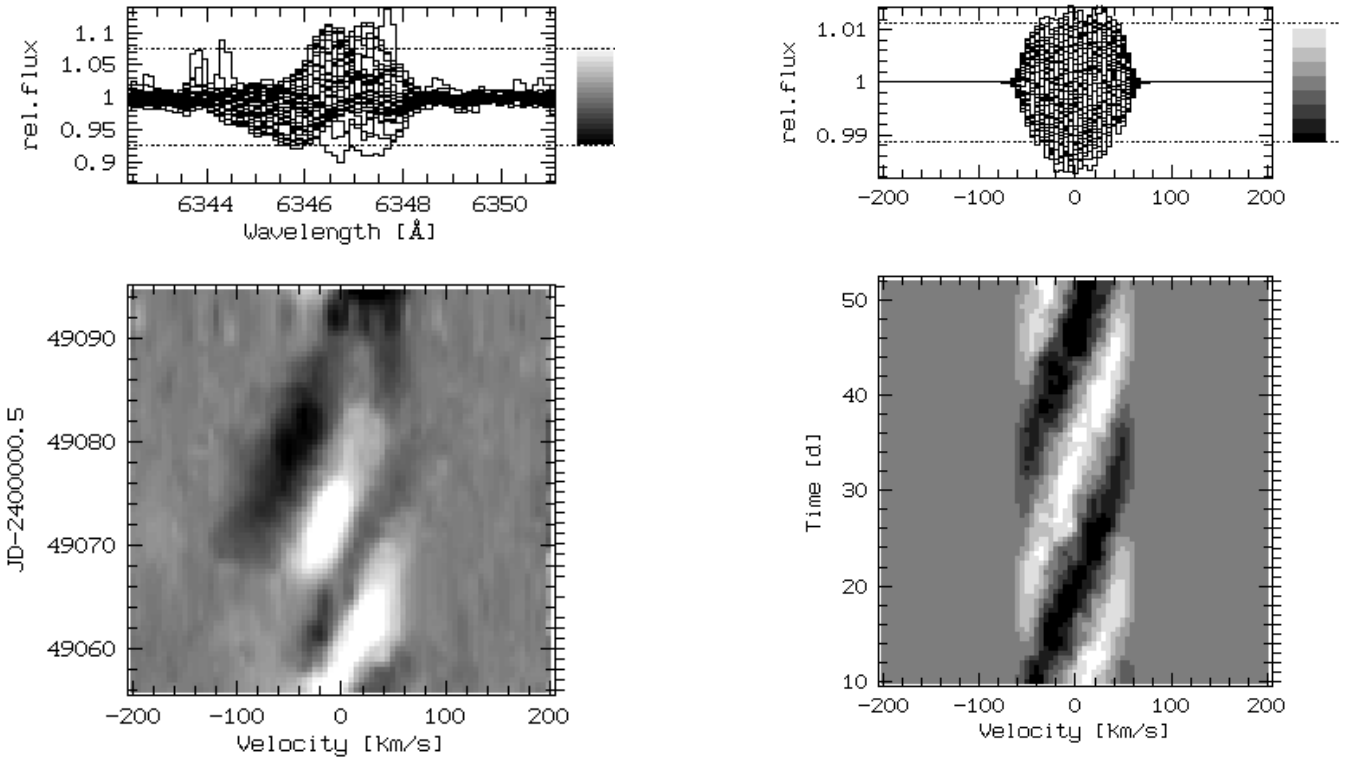

Fig. 11. Left: pseudo emissions- and pseudo absorption components, which travelled prograde across the quotient line profile of the Si IIλ6347 line of HD 92207 in 1993. These components are characteristic for non-radial pulsations in low modes. Since at one point in time one emission component is always visible together with one absorption component, the number of meridional sectors can be estimated to $|m| \approx 2$. Note that the spectra were shifted to laboratory wavelengths using a systemic velocity of $v_{\rm sys} = -17\,{\rm km\,s^{-1}}$ for HD 92207 (cf. Paper I, Table 4). Right: simulation of a non-radial pulsation with the stellar parameters of HD 92207 from Table 4 in Paper I and $\sin i = 1$, $l = -m = 2$, $\sigma_{\rm nrp} = \frac{2\pi}{60}\,{\rm d^{-1}}$. This leads to a measurable non-radial pulsation period of 27 d, which was also determined from the corresponding radial velocity curve and the LTPV photometry.

the variability of the numerous photospheric lines, which gives us detailed information on the temporal behaviour of the surface velocity fields.

An effective and precise cross-correlation method in connection with synthetic template spectra was used to measure the radial-velocity and line-strength curves of the metal-line spectrum. The radial-velocity curves show complex cyclical variations with a typical velocity dispersion of $\sigma \approx 3\,{\rm km\,s^{-1}}$. The corresponding line-strength variations, i.e., the equivalent-width variations, are less than 1% of the mean line strength if we assume a common modulation mechanism for both, radial velocities and line strengths. Such radial-velocity variations without significant changes of the equivalent widths are indicative of macroscopic velocity fields caused by non-radial pulsations with small amplitudes.

Furthermore, we do not find any depth dependence of the velocity field in the metallic lines (i.e., the Balmer lines excluded) of the BA-type supergiants in our sample. For α Cyg we find a systematic increase in the radial velocity of the Balmer lines from H27 to H8 by $3\,{\rm km\,s^{-1}}$, which we interpret as the onset of the radially accelerating velocity field of the stellar wind.

The CLEANed period spectra of the measured radial velocities of the metallic lines show the simultaneous excitation of multiple pulsation modes with periods longer and shorter than the estimated radial fundamental period of the objects, which might indicate the excitation of non-radial modes and radial overtones, respectively.

Periods derived from Strömgren photometry of HD 92207 coincide with the periods obtained from radial velocities. As suggested by the small color variations, the amplitudes of the light changes can be attributed largely to variations of the stellar radius.

The inspection of the LPV of the photospheric line spectrum reveals prograde travelling features in the dynamical spectra. The travelling times of these features are in contradiction to the possible rotation periods of these extended, slowly rotating objects. Therefore, we identify these features with non-radial pulsation modes, possibly g-modes, of low order ($l = |m| \lesssim 5$).

In addition to the multiplicity of the period spectra, the variability of the period spectrum from year to year complicates any precise determination of the pulsation modes, which is required in order to extract any asteroseismological information from the photospheric variability of these supergiants. Further, the

identification and theoretical handling of the acting excitation mechanisms is still not sufficiently clarified. Detailed period and amplitude spectra have to be derived from stellar models to allow a comparison with the observed photospheric variability.

7. Résumé

This series of three papers on the long-term spectroscopic monitoring of BA-type supergiants has revealed several interesting new aspects of the structure and variability of the extended circumstellar envelopes and the variable photospheric velocity fields of these luminous and massive hot stars. The research on the nature of the variability and its physical mechanisms is obviously still at the beginning. In general, the importance of the interaction of mass loss, rotation, magnetic fields and pulsation was made clear throughout this work by the analysis of extended spectroscopic time series with high resolution in wavelength and time. At this point, we would like to emphasize again that these unique data sets were obtained with telescopes of the sub-meter class.

Acknowledgements. We would like to thank the staff at La Silla Observatory for their kind assistance during the observations. This work was supported by the Deutsche Forschungsgemeinschaft (Wo 296/9-1, Wo 296/16-1,2).

References

Abt H., 1957, ApJ 126, 138
Achmad L., 1992, Depth of formation of spectral lines. In: de Jager C., Nieuwenhuijzen H. (eds.) Instabilities in evolved super- and hypergiants. Proceedings of the International Colloquium, Amsterdam, North-Holland, p. 42
Baschek B., Holweger H., Traving G., 1966, Abhandl. Hamburger Sternwarte 8, Nr. 1, 26
Burki G., 1978, A&A 65, 357
Chentsov E.L., Snezhko L.I., 1971, On differential shifts of lines in the spectrum of the supergiant β Ori. In: Hack M. (ed.) Proceedings of the Third Colloquium on Astrophysics, Trieste, 51
Fullerton A.W., Gies D.R., Bolton C.T., 1996, ApJS 103, 475
Gautschy A., 1992, MNRAS 259, 82
Groth H.G., 1972, A&A 21, 337
Kaufer A., Stahl O., Wolf B. et al., 1996a, A&A 305, 887 (Paper I)
Kaufer A., Stahl O., Wolf B. et al., 1996b, A&A 314, 599 (Paper II)
Kiriakidis M., Fricke K.J., Glatzel W., 1993, MNRAS 264, 50
Kurucz R.L., Peytremann E., 1975, A Table of Semiempirical gf Values, SAO Special Report 362, Cambridge
Kurucz R.L., 1979, ApJS 40, 1
Lovy D., Maeder A., Noëls A., Gabriel M., 1984, A&A 133, 307
Lucy L.B., 1976, ApJ 206, 499
Mehren S., 1994, Diploma thesis, Universitätssternwarte Göttingen
Paddock G.F., 1935, Lick Obs. Bull. 17, 99
Peytremann E., Baschek B., Holweger H., Traving G., 1967, Un Programme FORTRAN d'Analyse Quantitative de Spectre Stellaires, Obs. Genève
Rosendhal J.D., 1970a, ApJ 159, 107
Rosendhal J.D., Wegner G., 1970b, ApJ 162, 547
Stahl O., Kaufer A., Wolf B. et al., 1995, The Journal of Astronomical Data 1, 3
Sterken C., 1983, ESO Messenger 33, 10
Unno W., Osaki Y., Ando H., Shibahashi H., 1979, Nonradial Oscillations of stars, University of Tokyo Press, p. 30ff

This article was processed by the author using Springer-Verlag LaTeX A&A style file *L-AA* version 3.